Eur. Phys. J. A **23**, 201–215 (2005)
DOI 10.1140/epja/i2004-10079-7

THE EUROPEAN PHYSICAL JOURNAL A

Isomers in neutron-rich A ≈ 190 nuclides from ^{208}Pb fragmentation

M. Caamaño[1], P.M. Walker[1,2,a], P.H. Regan[1,3], M. Pfützner[4], Zs. Podolyák[1], J. Gerl[5], M. Hellström[5,6], P. Mayet[5,7], M.N. Mineva[6], A. Aprahamian[8], J. Benlliure[9], A.M. Bruce[10], P.A. Butler[11], D. Cortina Gil[5], D.M. Cullen[11,12], J. Döring[5], T. Enqvist[5,13], C. Fox[11,14], J. Garcés Narro[1], H. Geissel[5], W. Gelletly[1], J. Giovinazzo[15], M. Górska[5], H. Grawe[5], R. Grzywacz[16], A. Kleinböhl[5], W. Korten[17], M. Lewitowicz[18], R. Lucas[17], H. Mach[19], C.D. O'Leary[11], F. De Oliveira[18], C.J. Pearson[1], F. Rejmund[20], M. Rejmund[20], M. Sawicka[4], H. Schaffner[5], C. Schlegel[5], K. Schmidt[5], K.-H. Schmidt[5], P.D. Stevenson[1], Ch. Theisen[17], F. Vivès[5], D.D. Warner[21], C. Wheldon[1,5,11], H.J. Wollersheim[5], S. Wooding[1,5], F. Xu[1,22], and O. Yordanov[5]

[1] Department of Physics, University of Surrey, Guildford GU2 7XH, UK
[2] TRIUMF, 4004 Wesbrook Mall, Vancouver V6T 2A3, Canada
[3] Wright Nuclear Structure Laboratory, Yale University, New Haven, CT 06520, USA
[4] Institute of Experimental Physics, Warsaw University, PL-00681 Warsaw, Poland
[5] GSI, Planckstrasse 1, D-64291 Darmstadt, Germany
[6] Division of Nuclear Physics, Lund University, SE-22100, Sweden
[7] IKS, KU Leuven, Celestijnenlaan 200 D, B-3000 Leuven, Belgium
[8] Department of Physics, University of Notre Dame, South Bend, IN 46556, USA
[9] Departamento de Física de Partículas, University of Santiago de Compostela, 15706 Santiago de Compostela, Spain
[10] School of Engineering, University of Brighton, Brighton BN2 4GJ, UK
[11] Oliver Lodge Laboratory, University of Liverpool, Liverpool L69 7ZE, UK
[12] Schuster Laboratory, University of Manchester, Manchester M13 9PL, UK
[13] Department of Physics, University of Jyväskylä, 40351 Jyväskylä, Finland
[14] TUNL, Duke University, Durham, NC 27708-0308, USA
[15] CEN Bordeaux-Gradignan/CNRS, F-33175 Gradignan Cedex, France
[16] Department of Physics and Astronomy, University of Tennessee, Knoxville, TN 37996-1200, USA
[17] CEA Saclay, DSM/DAPNIA/SPhN, F-91191 Gif-sur-Yvette Cedex, France
[18] GANIL, BP 5027, F-14021 Caen Cedex, France
[19] Department of Radiation Sciences, Uppsala University, S-61182, Nyköping, Sweden
[20] IPN, 91406 Orsay Cedex, France
[21] CLRC Daresbury Laboratory, Warrington WA4 4AD, UK
[22] Department of Technical Physics, Peking University, Beijing 100871, PRC

Received: 21 July 2004 / Revised version: 10 September 2004 /
Published online: 7 December 2004 –
Communicated by J. Äystö

Abstract. Relativistic projectile fragmentation of ^{208}Pb has been used to produce isomers in neutron-rich, $A \approx 190$ nuclides. A forward-focusing spectrometer provided ion-by-ion mass and charge identification. The detection of γ-rays emitted by stopped ions has led to the assignment of isomers in ^{188}Ta, ^{190}W, ^{192}Re, ^{193}Re, ^{195}Os, ^{197}Ir, ^{198}Ir, ^{200}Pt, ^{201}Pt, ^{202}Pt and ^{203}Au, with half-lives ranging from approximately 10 ns to 1 ms. Tentative isomer information has been found also for ^{174}Er, ^{175}Er, ^{185}Hf, ^{191}Re, ^{194}Re and ^{199}Ir. In most cases, time-correlated, singles γ-ray events provided the first spectroscopic data on excited states for each nuclide. In ^{200}Pt and ^{201}Pt, the assignments are supported by γ-γ coincidences. Isomeric ratios provide additional information, such as half-life and transition energy constraints in particular cases. The level structures of the platinum isotopes are discussed, and comparisons are made with isomer systematics.

PACS. 21.10.Tg Lifetimes – 23.20.Lv γ transitions and level energies – 25.70.Mn Projectile and target fragmentation

1 Introduction

Projectile-fragmentation reactions at relativistic energies have been instrumental in the discovery of many exotic nuclides in their ground state [1–3]. The observation of γ radiation, following isomer decay within a microsecond time range after fragment detection, provides a sensitive means to identify corresponding excited states. The γ-ray spectra can be associated with individual nuclides, and

[a] e-mail: p.walker@surrey.ac.uk

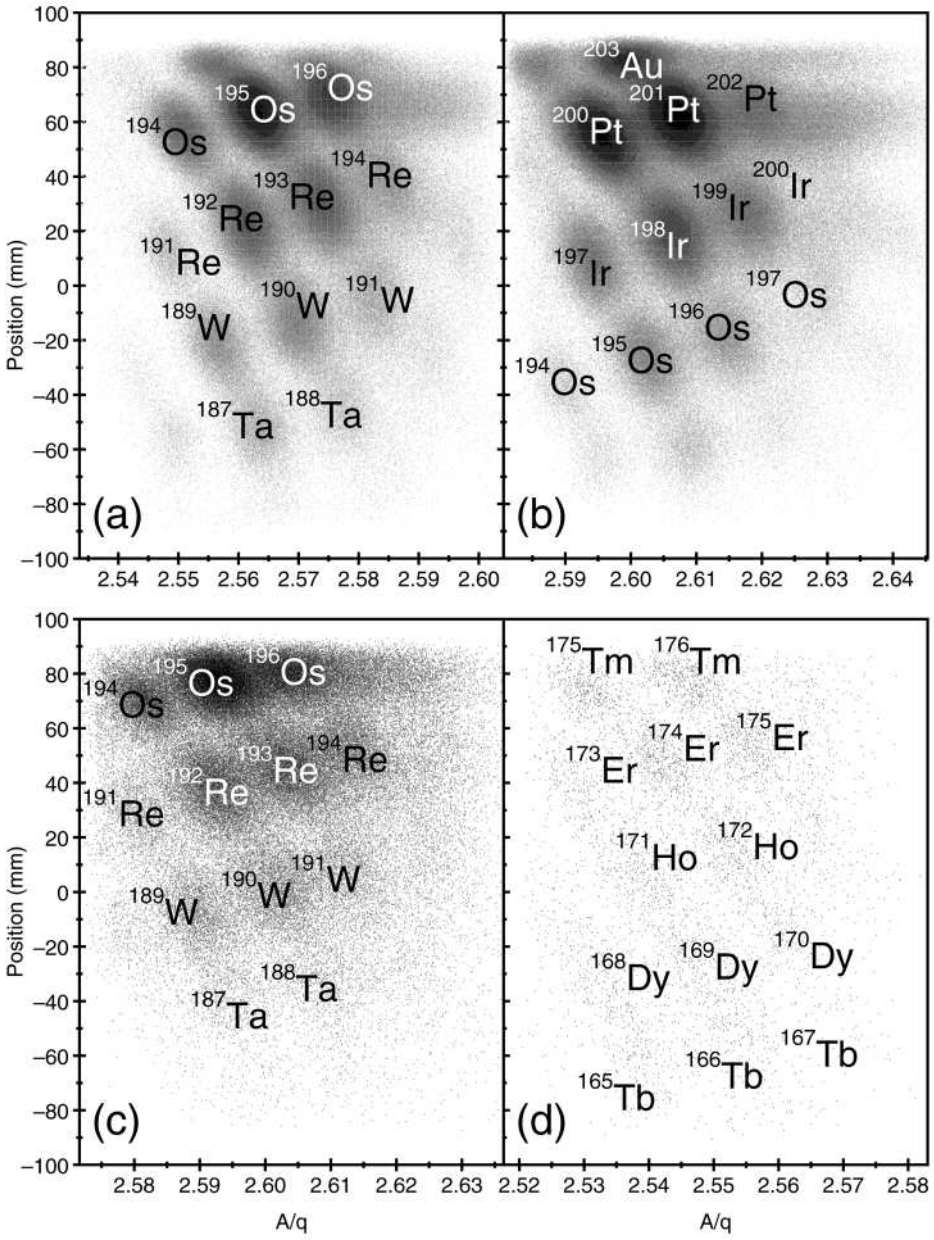

Fig. 1. Ion-identification plots, in terms of focal-plane position *versus* A/q, following ^{208}Pb fragmentation: (a) ^{191}W setting, fully stripped ions; (b) ^{191}W setting, hydrogen-like ions; (c) ^{184}Lu setting, hydrogen-like ions; (d) ^{170}Dy setting, fully stripped ions. See text for additional explanation. Note that the events labelled as ^{197}Os and ^{200}Ir in (b), and ^{170}Dy in (d), correspond to previously unreported nuclides.

many nuclides can be studied simultaneously with a single spectrometer setting. This method has previously been applied successfully to make new isomer discoveries in medium-mass nuclides at GANIL [4–10] and heavy nuclides at GSI [11–14].

The present work is concerned with the neutron-rich, $A \approx 190$ region of the nuclide chart, which until recently has remained largely unexplored, although there have been several theoretical predictions of multi-quasiparticle, isomeric states [15–17]. Advances in the development of nuclear spectrometers, and associated γ-ray detection techniques, have opened up new experimental possibilities.

In the following sections, we report results obtained from ^{208}Pb projectile-fragmentation reactions. Many of these results, now presented systematically, have been previously reported in preliminary form [18–28]. The neutron-rich, $A \approx 190$ nuclides that have been studied span a range of intrinsic and collective structures, from prolate-deformed through triaxial to spherical shapes with increasing mass number. Closely related work on spin distributions, obtained by studying known $A \approx 180$ isomers

with the same experimental equipment, has been reported by Pfützner *et al.* [14,29].

2 Experimental technique

The nuclides of interest were produced in the interaction of a ^{208}Pb primary beam at 1 GeV per nucleon, from the SIS heavy-ion synchrotron at GSI, with a 1.6 g/cm^2 beryllium target located at the entrance of the Fragment Separator (FRS) [30]. The average primary beam intensity, as measured by a secondary electron monitor (SEETRAM), varied between 1×10^6 ions per spill, when fragments close to the projectile mass were selected, and 2×10^8 ions per spill at settings for nuclides far from the line of stability. The typical length and repetition period of a spill were 4 and 10 seconds, respectively. The FRS was operated in standard achromatic mode [30] with an aluminium wedge-shaped degrader at the intermediate focal plane. Niobium foils of thickness 221 mg/cm^2 and 108 mg/cm^2 were mounted downstream from the target and degrader, respectively, in order to increase the electron-stripping cross-section. The probability of an ion being fully stripped of electrons in the first and second sections of the FRS was calculated, using the electron-stripping code GLOBAL [31], to be about 96% and 88%, respectively. The experimental setup included two multi-wire proportional counters, for position measurements; two scintillation detectors, providing time-of-flight and position information; and a further two scintillators and an ionisation chamber (MUSIC) for energy loss measurements. Fragments were eventually stopped at the final focal plane in an inclined aluminium plate, which was placed between four clover germanium detectors (providing sixteen independent germanium crystals) with 6% absolute full-energy-peak efficiency at 1.3 MeV, as measured with ^{60}Co and ^{152}Eu radioactive sources.

The particle-identification procedure is described in detail in ref. [14]. Ion-by-ion mass number (A) and proton number (Z) identification was achieved in terms of focal-plane position *versus* A/q, where q is the ionic charge, as illustrated in fig. 1. Events from ions passing through the second time-of-flight scintillator were then time-correlated with γ-ray energies measured in the germanium detectors. For each germanium crystal, the energy and time of the first γ-ray event was recorded after the arrival of a heavy ion, up to a maximum time of 75 μs.

The basic FRS settings selected were those that correspond approximately to the central transmission of fully stripped ions of ^{174}Yb, ^{184}Lu, ^{191}W and ^{170}Dy. These nuclides are therefore used as convenient labels to specify the settings, which involved data collection times of approximately 10, 30, 50 and 40 hours, respectively. Although the vast majority of events correspond to well-defined charge states, it should be noted that the FRS selection is actually dependent on the charge-changing properties of each ion. Thus "fully stripped" ions correspond to no charge state change between the first and second sections of the FRS, while "hydrogen-like" ions correspond to the pick-up of one electron at the intermediate focal plane, and "helium-like" ions correspond to the pick-up of two electrons. Since the fully stripped fraction in the first section is large (in the present instance about 96%) there is no significant problem with charge state ambiguities. Therefore, we will continue to refer to the dominant charge state in the second section of the FRS when discussing the different ion groups, with the proviso that a few percent of the ions have additional electrons and, consequently, different A and Z.

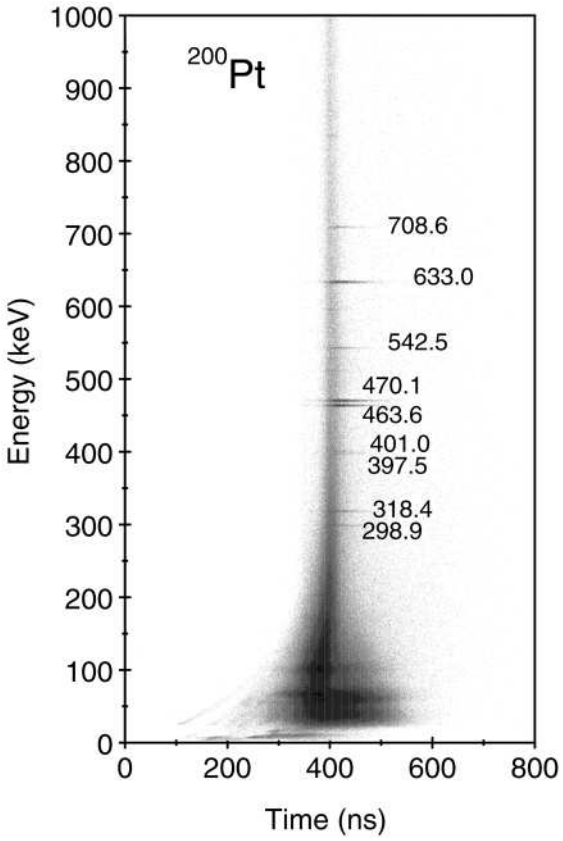

Fig. 2. Energy *versus* time for ^{200}Pt events. The time axis has an arbitrary zero. See text for discussion.

Reference points for nuclide identification (and hence A and Z calibration) were obtained primarily by recognising the energies of γ-rays from the decays of known isomers in ^{200}Pt [32] and ^{206}Hg [33]. The γ-ray events were incremented into energy *versus* time matrices. For ^{206}Hg the known 2 μs, $J^\pi = 5^-$ isomer was evident, though the recently reported higher-spin isomeric decays [34,35] were not observed in the present work. Figure 2 shows the ^{200}Pt data.

Since the known isomer in ^{200}Pt is short lived (14 ns [32]) the analysis of the time evolution is now discussed. The half-life was determined for particular γ-ray transitions by first fitting a Gaussian peak shape to the time spectrum of adjacent continuum background events (as shown by the dot-dashed line in fig. 3) to obtain a value for the "prompt" width and centroid. Note that there is no *a priori* definition of the γ-ray arrival time relative to the associated ion, that would establish the "zero" of the time axis. The assumed "prompt" events in the germanium detectors are understood to come predominantly

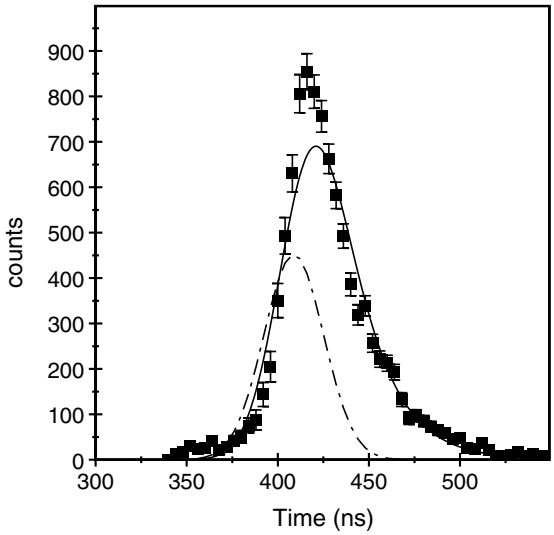

Fig. 3. Half-life fit for ^{200}Pt, yielding 14.0 ± 0.6 ns, from time projections of the 464 and 470 keV γ-ray transitions. The Gaussian curve (dot-dashed line) shows the "prompt" peak shape (FWHM = 39 ns). See text for discussion.

from charged particles and bremsstrahlung, generated as the ions are slowed and stopped. In order to obtain a half-life measurement for the background-subtracted γ-ray peak events, the fitted Gaussian shape was convoluted with an exponential decay (continuous line and data points in fig. 3). The measured half-life of 14.0 ± 0.6 ns is in good agreement with that obtained by Yates *et al.* [32] (14.3 ± 0.6 ns) for the $J^\pi = 7^-$ isomer in ^{200}Pt. The survival of such a short-lived isomer through the FRS, with a flight time of approximately 300 ns, depends on the suppression of electron conversion for highly stripped ions, *i.e.* the in-flight ionic half-life is substantially longer than the neutral-atom half-life, the latter being what is measured at the aluminium stopper. In the present case, the isomer decays by an $E2$ transition of energy ≤ 100 keV [32], so that the total conversion coefficient [36] is $\alpha_{\rm tot} \geq 5$ and the fully stripped, in-flight half-life is ≥ 85 ns. Furthermore, since each ^{200}Pt ion carries one or two K-shell electrons, which could enable in-flight decay by electron conversion, it is additionally required that the transition energy is less than the one-electron K-binding energy of 90 keV [37] (see also sect. 4). The other transitions and the level structure of ^{200}Pt are discussed in sect. 3.

It is apparent from fig. 3 that the procedure for obtaining the "prompt" peak shape from the continuum slightly overestimates the time width of the discrete γ-ray transitions. This is an issue of some interest, perhaps related to a significant time distribution of continuum (bremsstrahlung) events, as well as the Compton-scattered events having a different time response to the full-energy events. However, there are no "prompt" discrete transitions with which to define the true time resolution. Nevertheless, the exponential half-life component thus obtained agrees with the known value, as discussed above.

3 Results

The isomer data are summarised in table 1. First, we discuss the framework within which the results are presented. Projections of energy-*versus*-time matrices were made for each nuclide. Representative γ-ray energy and time spectra are shown in the following sections. Energies and half-lives were used to calculate Weisskopf hindrance factors, $F_{\rm W}$ (allowing for electron conversion) to give a consistent indication of transition multipolarities, by comparison with the systematics of Löbner [38]. The X-ray intensities, and γ-ray intensity balances, provide additional valuable constraints on conversion coefficients.

Isomeric ratios have been calculated, *i.e.* the ratio of the number of ions of a given nuclide in an isomeric state to the total number of ions of that nuclide. The methodology is discussed in detail in our previous paper [14], where critical evaluation is given of the sharp-cutoff model of angular-momentum generation in fragmentation reactions. Here, the purpose is three-fold: i) for long half-lives, isomeric ratios can provide useful half-life upper limits; ii) for short half-lives, where extended in-flight half-lives are implied, isomeric ratios constrain the electron conversion coefficients, and hence provide transition-energy upper limits; and iii) isomeric ratios can be used in planning future experiments.

In the following sections, the principal results for individual nuclides are presented in order of increasing mass number. For the first case, ^{188}Ta, some additional information is included, to illustrate the methodology. Furthermore, tentative evidence for isomers in ^{174}Er, ^{175}Er, ^{185}Hf, ^{191}Re, ^{194}Re and ^{199}Ir is presented at the end of sect. 3.

3.1 $^{188}_{73}$Ta$_{115}$

The energy and time spectra in fig. 4 (top) represent the first spectroscopic data obtained for excited states of ^{188}Ta. These spectra are each the sum of three spectra obtained from three different experimental conditions (see fig. 5). A half-life of 5 ± 2 μs (shown in fig. 4 insert) was calculated by fitting an exponential decay to the time projection of the 292 keV transition.

To interpret the 292 keV γ-ray transition, it is first assumed that, as only one transition was observed, it is likely to be the direct decay from the isomeric state, though there is also the possibility that there is an unobserved, low-energy transition depopulating the isomer (see below). Hindrance factors indicate that the 292 keV transition, if it comes directly from the 5 μs isomer, could have multipolarity $E2$ ($t^{\rm W}_{1/2} = 4$ ns, $F_{\rm W} = 1.3 \times 10^3$) or $M2$ ($t^{\rm W}_{1/2} = 0.5\,\mu$s, $F_{\rm W} = 22$). The Weisskopf half-life estimates quoted here are not corrected for internal conversion, although the hindrance factors are —this is the convention adopted in all the following half-life and hindrance comparisons. The possibility of the transition being of $M2$ character is, however, ruled out. If this were the case, the 292 keV transition would have a K-electron conversion coefficient of $\alpha_K = 0.72$, and 58 keV tantalum X-rays,

Table 1. Summary of isomer results, giving γ-ray (and X-ray) transition energies and intensities, percentage isomeric ratios, tentative J^π assignments, half-lives and FRS settings.

	E_γ(keV)	I_γ [a]	$IR^{\rm exp}$ [b]	$IR^{\rm sc}$	J^π	$t_{1/2}$ [c]	S [d]	CS [e]
^{188}Ta	292.4 ± 0.2	96 ± 12	$0.5^{+0.3}_{-0.1}$			5 ± 2 μs	^{191}W	F
							^{184}Lu	F+H
^{190}W	58.5 ± 0.5	60 ± 13	> 2	30	10^-	60^{+1500}_{-30} μs	^{191}W	F
	207.0 ± 0.3	27 ± 7					^{184}Lu	H
	357.4 ± 0.3	24 ± 7						
	484.0 ± 0.4	21 ± 7						
	593.6 ± 1.1	21 ± 8						
	694.0 ± 0.7	16 ± 7						
^{192}Re	60.6 ± 0.2	550 ± 45	21^{+29}_{-7}			120^{+210}_{-50} μs	^{191}W	F+H
	69.5 ± 0.4	154 ± 31					^{184}Lu	H
	160.1 ± 0.2	526 ± 40						
^{193}Re	60.6 ± 0.2	989 ± 58	> 19			75^{+450}_{-40} μs	^{191}W	F+H
	69.5 ± 0.3	247 ± 35					^{184}Lu	H
	146.1 ± 0.3	135 ± 26						
^{195}Os	438.6 ± 0.2	365 ± 53	> 13			26 ± 4 ns	^{191}W	F
	493.0 ± 0.2	266 ± 44						
	533.1 ± 0.2	355 ± 57						
	714.0 ± 0.3	364 ± 59						
^{197}Ir	161.0 ± 0.5	39 ± 14	2.0 ± 0.2			30 ± 8 μs	^{191}W	H
	278.5 ± 0.2	91 ± 17						
	378.8 ± 0.2	78 ± 17						
	458.3 ± 0.5	53 ± 16	1.0 ± 0.1			15 ± 9 μs		
	495.0 ± 0.3	67 ± 17						
	567.1 ± 0.3	69 ± 17						
	609.1 ± 0.5	24 ± 12						
^{198}Ir	116.4 ± 0.2	481 ± 30	19^{+5}_{-3}			77 ± 9 ns	^{191}W	H
^{200}Pt	298.9 ± 0.2	851 ± 98	> 25	36	7^-	14.0 ± 0.6 ns [f]	^{191}W	H+He
	318.4 ± 0.2	1530 ± 104						
	397.5 ± 0.2	556 ± 81						
	401.0 ± 0.2	558 ± 84						
	463.6 ± 0.2	7042 ± 173						
	470.1 ± 0.2	7803 ± 179						
	542.5 ± 0.2	1070 ± 84	> 4	8	12^+	10.3 ± 2.4 ns		
	633.0 ± 0.2	7223 ± 187						
	708.6 ± 0.2	1546 ± 108						
^{201}Pt	354.1 ± 0.2	984 ± 60	> 32	30	$\frac{19}{2}^+$	21 ± 3 ns	^{191}W	H+He
	374.4 ± 0.2	1034 ± 62						
	727.2 ± 0.2	931 ± 70						
^{202}Pt	534.9 ± 0.2	226 ± 29	> 15	35	7^-	280^{+420}_{-190} μs	^{191}W	H+He
	718.7 ± 0.2	123 ± 25						
^{203}Au	563.3 ± 0.3	74 ± 17	> 1			40^{+7000}_{-20} μs	^{191}W	He

[a] Relative γ-ray intensity during the 75 μs recording interval; where available, X-ray energies and intensities are also given. These are efficiency-corrected counts, in the obtained γ-ray spectra, with arbitrary overall normalisation.

[b] The isomeric ratio is given as a percentage of the total number of ions. Both the experimental values (exp) and the corresponding upper-limit estimates from the sharp-cutoff model (sc) are given. The lower limits for experimental values result from half-lives that are either very short or very long (see text for details).

[c] Half-lives are for ions at rest, measured at the final focus of the FRS.

[d] Nominal FRS setting for optimal transmission of fully-stripped ions.

[e] Transmitted charge states: F (fully-stripped), H (hydrogen-like) and He (helium-like).

[f] The literature value for ^{200}Pt (7^-) is 14.3 ± 0.6 ns [32].

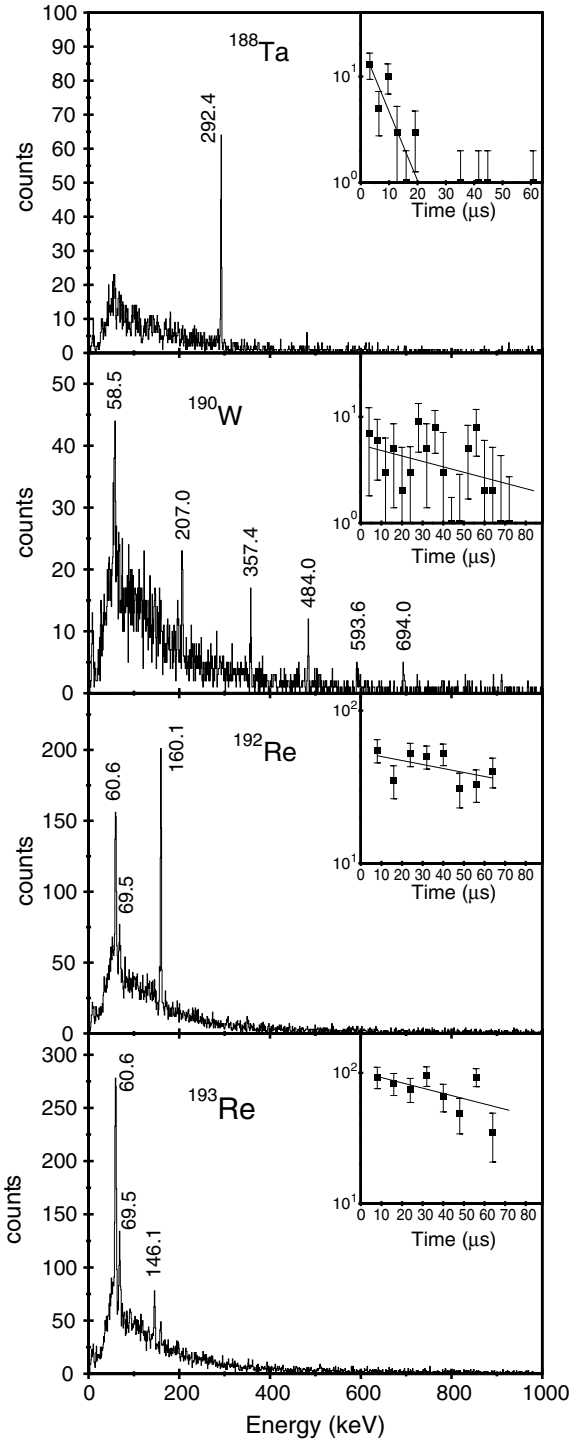

Fig. 4. Gamma-ray energy spectra taken over the 1–75 μs time interval for (top to bottom) ^{188}Ta, ^{190}W, ^{192}Re and ^{193}Re. The inserts show the half-life fits of (respectively) 5 ± 2 μs, 60^{+1500}_{-30} μs, 120^{+210}_{-50} μs and 75^{+300}_{-40} μs.

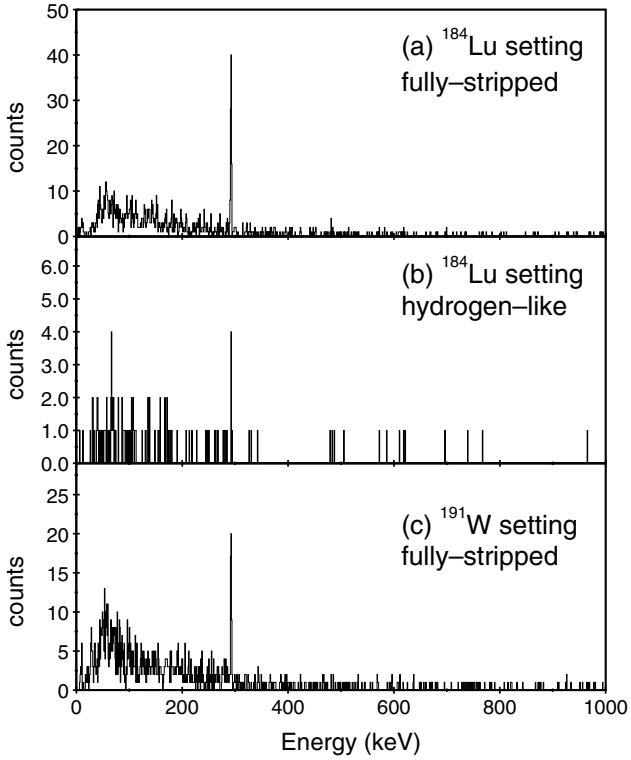

Fig. 5. The final ^{188}Ta γ-ray energy spectrum (fig. 4) is the sum of the spectra from (a) and (b), the fully stripped and hydrogen-like ions from the ^{184}Lu setting, and (c) the fully stripped ions from the ^{191}W setting.

with an intensity approximately equal to 70% of the γ-ray peak, would be expected, contrary to observation (cf. spectra discussed later, where X-rays can be seen).

There could also be an unobserved, low-energy transition, depopulating the isomer. This ($E \leq 50$ keV) transition could then have $E1$ character, with $t^{\mathrm{W}}_{1/2} = 2$ ps at 50 keV, and $F_{\mathrm{W}} = 5 \times 10^6$. Large hindrance factors like this are typical for $E1$ transitions [38]. In this scenario, the 292 keV transition could be the first cascade transition of a rotational band. The corresponding $M1$ conversion coefficient is $\alpha_K = 0.19$, which is consistent with the experimental photon intensity limit in the X-ray region (and also consistent with $E2$ admixture).

It is appropriate to comment on the "$E \leq 50$ keV" designation. This limit is below the K-electron binding energy of 67 keV for tantalum, so that K X-ray production, via electron conversion, would not be involved. Nevertheless, higher-shell conversion reduces the γ-ray intensity. Furthermore, the γ-ray detection efficiency falls rapidly for energies below 50 keV. As a consequence, the γ-ray detectors were insensitive to transitions with energies below 50 keV.

The level to which the 292 keV transition decays could itself be an isomer. In that case, at least one of the following conditions would need to be satisfied: i) its half-life is greater than 1 ms, and/or ii) its excitation energy is less than 50 keV. In either case, the present experimental arrangement would be insensitive to the corresponding isomeric decay. A similar situation applies in principle to all of the odd-odd and odd-mass nuclides that are discussed in the following sections, *i.e.* the lowest level "observed" is not necessarily the ground state.

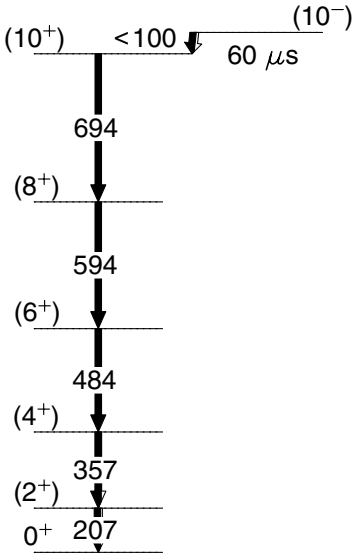

Fig. 6. Proposed level scheme for ^{190}W. Spins and parities are derived from systematics.

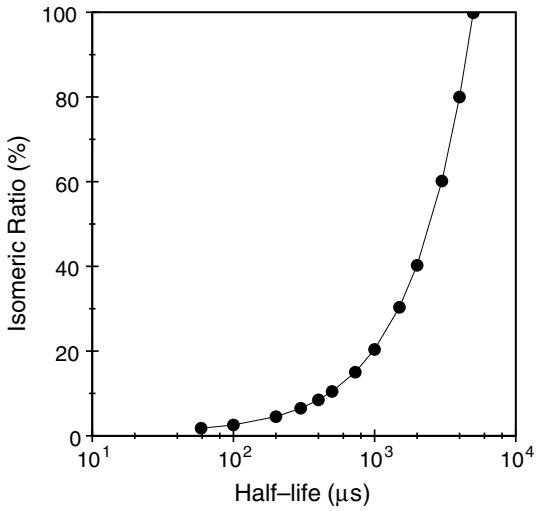

Fig. 7. Isomeric ratio analysis for determination of the half-life upper limit of the ^{190}W isomer. A range of half-lives was used to calculate the corresponding isomeric ratios. The implied isomeric ratio increases with half-life because the measuring time is limited to 75 μs after the arrival of each ion.

3.2 $^{190}_{74}$W$_{116}$

Figure 4 shows the γ-ray energy and time spectra obtained by projecting energy-*versus*-time matrices, constituting the first evidence for excited states observed in ^{190}W. The X-ray peak at 58.5 keV reinforces the particle identification by confirming that the excitations observed are those of a tungsten isotope. Although statistics were not good enough to allow for γ-γ coincidences, a partial level scheme is proposed (fig. 6) based on systematics of even-even tungsten nuclei in this mass region [39] (see also sect. 4). It is suggested that the γ-ray transitions observed have $E2$ character and form a rotational cascade built on the ground state, as we reported previously [12]. (The 593.6±1.1 keV transition energy differs from the previously quoted value of 591 keV, due to the combination of including additional channels in the peak region, and the modified sorting conditions discussed below.)

The half-life of the isomer was deduced by first fitting an exponential decay to the time projection of the sum of the peaks at 207, 357 and 484 keV (refer to fig. 4). The best fit gives a half-life of 60 μs, and a χ^2 analysis gives a lower limit of 30 μs, but no upper limit. The isomeric ratio can, however, be used to specify an upper limit, based on the events that are observed over the 75 μs time range. Had all the ^{190}W nuclei been produced in the isomeric state, then the maximum possible isomeric ratio would be 100% (by definition). Figure 7 shows half-life values plotted against corresponding values of isomeric ratio for this nuclide. The 100% limit gives a maximum half-life value of 5 ms, so $t_{1/2} = 60^{+4900}_{-30}$ μs. We note that this differs from our earlier value of 270^{+3000}_{-180} μs [12]. The difference arises from independent analyses of the data (see also comments below) and, in view of the very large statistical uncertainties involved, is not considered to be significant. If, furthermore, we adopt the maximum isomeric ratio of 30%, as calculated using the sharp-cutoff model [40] discussed in sect. 4, then $t_{1/2} = 60^{+1500}_{-30}$ μs is obtained.

As has been presented earlier [12], multi-quasiparticle calculations suggest that a low-lying, 2-quasi-neutron, $K^\pi = 10^-$ isomeric state, with Nilsson configuration $\frac{9}{2}^-[505]\downarrow\nu \otimes \frac{11}{2}^+[615]\uparrow\nu$, is feeding the rotational band. This is the same configuration as the 5.9 s isomer in the $N = 116$ isotone ^{192}Os and the 9.9 m isomer in ^{190}Os [39]. This assignment would imply that the isomeric level is depopulated by an $E1$ transition, which would be highly K forbidden. In our previous publication on this nucleus [12] a 46 keV transition was proposed for this $E1$ decay. However, a re-analysis of the data makes this assignment uncertain, as the 46 keV peak appears only to have significant intensity in particular germanium crystals. Indeed, if one of these crystals is removed from the sort program, then the resultant γ-ray spectrum is that shown in fig. 4, and the 46 keV transition is no longer statistically significant. Accordingly, the decay from the proposed 10^- isomer requires further discussion. The depopulating transition should have $E_\gamma \leq 100$ keV for an $E1$ transition ($t^{\rm W}_{1/2} = 0.2$ ps at 100 keV, $F_{\rm W} \sim 4 \times 10^8$) otherwise a corresponding peak should be clearly observable in the γ-ray spectrum. The rather large intensity of the tungsten K X-rays seems to imply that any proposed $E1$ transition should have an energy just above the K-electron binding energy (69.5 keV) and $\alpha_{\rm tot} \approx 1$ (*e.g.* $\alpha_{\rm tot} = 0.91$ for a 71 keV transition). Another possibility is that the $E1$ transition energy has a chance equality with the K X-ray energy, so that the intensity of the 58.5 keV peak is part γ-ray, part X-ray.

3.3 $^{192}_{75}$Re$_{117}$

The results shown in fig. 4 represent the first spectroscopic data available for excited states of ^{192}Re. The lower-energy peaks at 60.6 and 69.5 keV are the rhenium K_α and K_β

X-rays, respectively, clearly identifying the element as rhenium. The half-life is determined to be 120^{+210}_{-50} μs. If the observed 160 keV γ-ray is the direct de-excitation from an isomeric level, then it is likely to have $E2$ ($t^{\rm W}_{1/2} = 80$ ns, $F_{\rm W} = 2\times10^3$) or $M2$ ($t^{\rm W}_{1/2} = 9$ μs, $F_{\rm W} = 130$) multipolarity. However, on examination of X-ray and γ-ray relative intensities, as well as conversion coefficients, an $M1$ decay ($\alpha_K = 1.2$) appears to be the most likely. This is because $\alpha_K = 0.3$ for an $E2$ transition, implying 60% less intense X-rays than those observed. An $M2$ transition, on the other hand, would have $\alpha_K = 6.3$, requiring six times more intense X-rays. Hindrance factors suggest, however, that an $M1$ decay would be strongly hindered ($F_{\rm W} = 5\times10^7$). We therefore infer that the 160 keV transition may not be the direct decay from the isomeric level, but rather may depopulate a state that is fed by an unobserved low-energy (≤ 50 keV) $E1$ transition ($F_{\rm W} = 10^8$ at 50 keV).

3.4 $^{193}_{75}$Re$_{118}$

The results shown in fig. 4 represent the first spectroscopic data obtained for excited states of ^{193}Re. The K_α and K_β X-rays are clearly visible. Only one γ-ray transition was observed, at 146.1 keV, with slight contamination from the 160.1 keV transition in ^{192}Re. (The issue of adjacent-nuclide contamination is discussed in more detail in sect. 3.9.) From the time dependence of the X-ray intensity, the half-life of the isomer is found to be 75^{+450}_{-40} μs, the upper limit corresponding to the maximum isomeric ratio of 100%.

Hindrance factors indicate that the 146 keV transition is likely to have $M2$ ($t^{\rm W}_{1/2} = 14$ μs, $F_{\rm W} = 70$) or $E2$ ($t^{\rm W}_{1/2} = 0.1$ μs, $F_{\rm W} = 10^3$) multipolarity, if the assumption is made that it is the direct decay from an isomeric state. The high intensity of the X-rays supports an $M2$ assignment.

3.5 $^{195}_{76}$Os$_{119}$

The data shown in fig. 8, with γ-ray transition energies of 439, 493, 533 and 714 keV, constitute the first spectroscopic evidence for excited states in ^{195}Os. The isomer half-life of 26 ± 4 ns is determined by fitting the time dependence of the γ-ray intensity with a convolution of Gaussian and exponential functions. Because the isomer half-life is short, it is not possible to separate completely the isomeric γ-rays from the low-energy (bremsstrahlung) background in the spectrum, precluding the possibility of identifying any X-rays or γ-ray transitions below about 300 keV.

There are insufficient statistics to determine γ-γ coincidences in this work, but a recent deep-inelastic reaction measurement has shown that the four transitions are in mutual coincidence [41]. The 439, 493 and 533 keV transitions appear to be in a collective cascade because they have similar intensities (see table 1) and are spaced at regular intervals, but the 714 keV transition may originate from a different intrinsic structure. However, the 714 keV transition cannot be the transition that directly de-excites the 26 ns isomer. This is because, due to its high energy, its conversion coefficient would be small and, correspondingly, the in-flight half-life would be too short to permit the survival of the isomer through the FRS. The limitations on the energy of the directly depopulating transition are discussed in sect. 4.

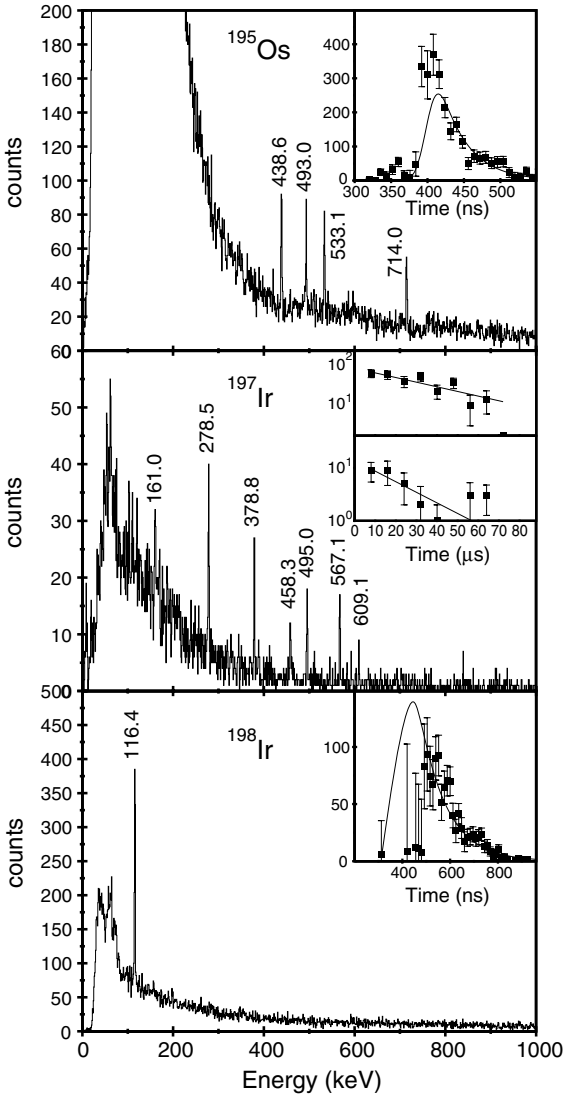

Fig. 8. Gamma-ray energy spectra for (top to bottom) ^{195}Os, taken with a 60 ns time cut; ^{197}Ir, for the time region 1–75 μs; and ^{198}Ir, with a 500 ns time cut (excluding prompt events). The inserts show the corresponding time spectra with (top to bottom) half-lives of 26 ± 4 ns, 30 ± 8 μs (upper insert for the sum of the 278.5, 378.8, 495.0 and 567.1 keV transitions), 15 ± 9 μs (lower insert for 458.3 keV transition), and 77 ± 9 ns. For the last case there is a poor fit in the prompt region, where the data have large error bars on account of the subtracted background, but this has no significant effect on the fitted half-life.

3.6 $^{197}_{77}$Ir$_{120}$

Cizewski *et al.* [42] assigned spins and parities to several excited states that they observed in ^{197}Ir using the

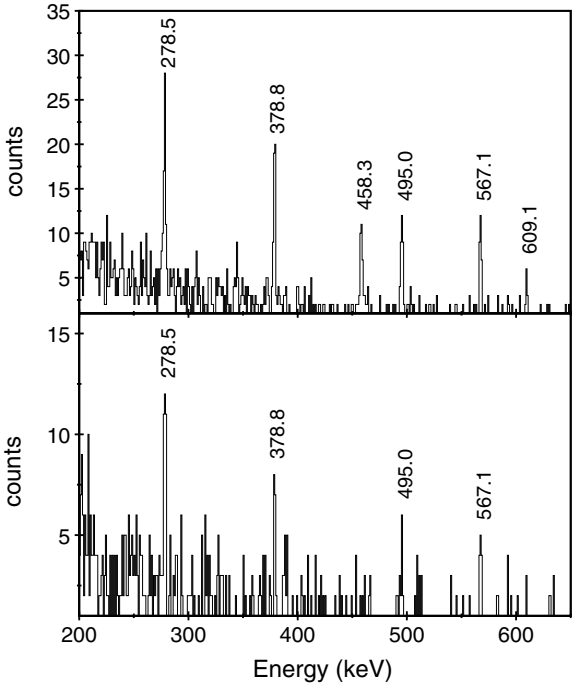

Fig. 9. Gamma-ray energy spectra over two sequential 37 μs intervals, showing evidence for two isomers in ^{197}Ir (the 458.3 keV transition apparently having a shorter half-life).

^{198}Pt$(\mathbf{t},\alpha)^{197}$Ir reaction. Their excitation energies at 460, 495, 561 and 606 keV, with an uncertainty of $\pm$ 5 keV, are consistent with γ-ray transition energies observed in this work, *i.e.* those at 458.3, 495.0, 567.1 and 609.1 keV (see fig. 8) and some of these associations may be significant. However, in the absence of sufficient γ-ray coincidence data, we are unable to establish a reliable level structure.

The intensities of the γ-ray peaks in fig. 8 are non-uniform, indicating the possibility of there being more than one cascade, and hence more than one isomer. Figure 9 illustrates energy spectra with two different time gates, supporting this suggestion. The time spectra (see fig. 8 inserts) give half-lives of 30 ± 8 μs and 15 ± 9 μs.

3.7 $^{198}_{77}$Ir$_{121}$

A single transition, at 116 keV, with a half-life of 77$\pm$9 ns, was identified in ^{198}Ir (see fig. 8), constituting the first spectroscopic data recorded for excited states of this nuclide. Hindrance factors suggest that if the 116 keV transition is directly depopulating an isomer, it is likely to have $E1$ multipolarity ($t^{\rm W}_{1/2} = 0.1$ ps, $F_{\rm W} = 8\times10^5$, $\alpha_K = 0.22$) and this is supported by the lack of observed X-ray events.

3.8 $^{200}_{78}$Pt$_{122}$

The structure of ^{200}Pt, from the ^{198}Pt(t,p) reaction, has been studied by Cizewski *et al.* [43] and Yates *et al.* [32]. We have observed some of the γ-ray transitions reported

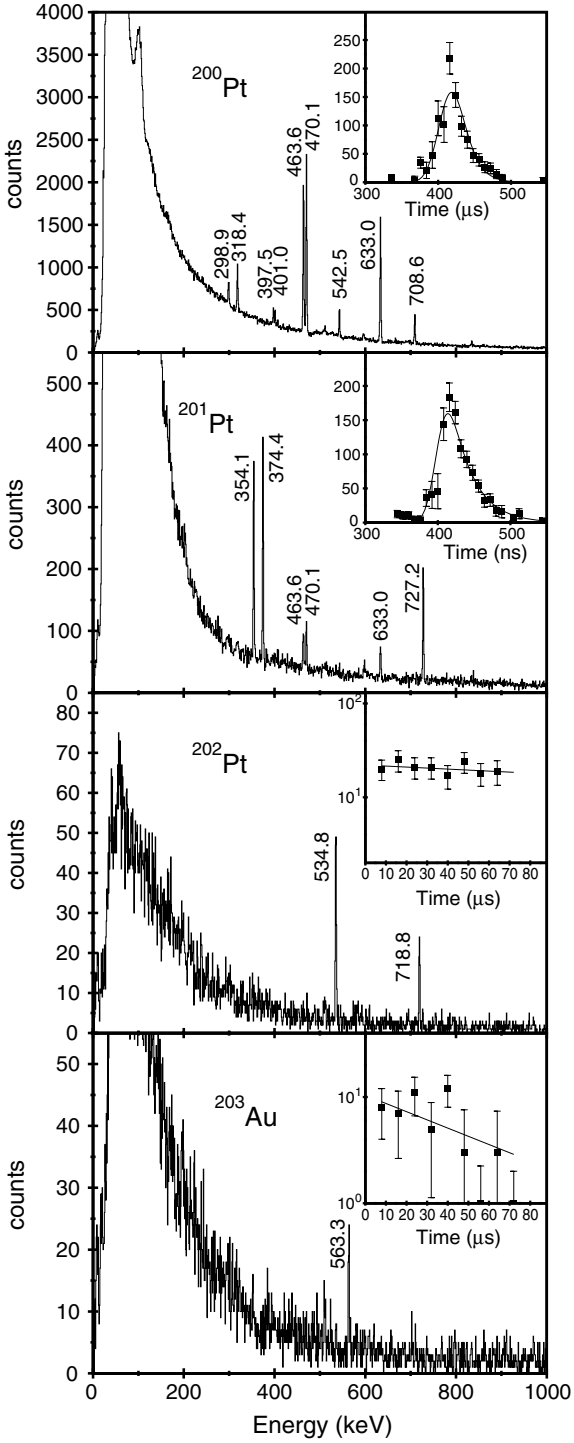

Fig. 10. Gamma-ray energy spectra for (top to bottom) ^{200}Pt, with a 180 ns time cut (including prompt events) where the γ-rays at 542.5 and 708.6 keV are previously unreported; ^{201}Pt, from a 70 ns time cut (peaks at 463.6, 470.1 and 633.0 keV are contamination from ^{200}Pt); ^{202}Pt, over the 1–75 μs time interval; and ^{203}Au, over the 5–75 μs time interval. The inserts show corresponding time spectra with, respectively, fitted half-lives of 10.3 ± 2.4 ns (upper isomer —see fig. 3 for the lower isomer), 21 ± 3 ns, 280^{+420}_{-190} μs, and 40^{+7000}_{-20} μs.

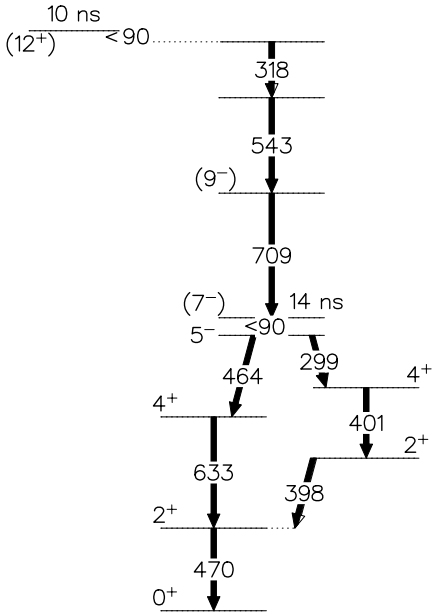

Fig. 11. Proposed level scheme for ^{200}Pt. The assignments up to the 14 ns isomer are from Yates *et al.* [32]. The ordering of the 709, 543 and 318 keV transitions cannot be determined in the current work (see text).

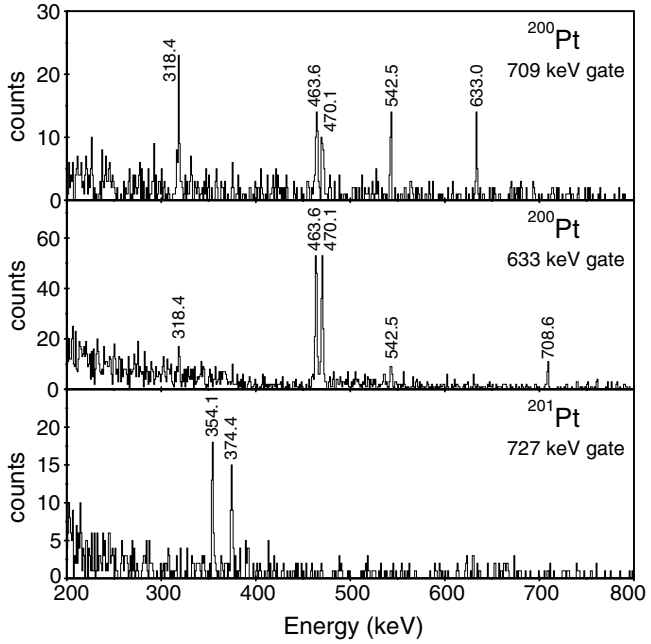

Fig. 12. Examples of γ-γ coincidence spectra for ^{200,201}Pt. The 318.4, 542.5 and 708.6 keV transitions in ^{200}Pt are seen to be in coincidence with known transitions. The three transitions in ^{201}Pt are all in mutual coincidence.

by Yates *et al.*, and at least two more that they did not observe, illustrated in fig. 10. The level scheme for ^{200}Pt has now been extended to include a previously unreported isomer (see fig. 11).

In this case, γ-γ coincidence gating was informative (see fig. 12). There are found to be two isomers, both short lived ($\sim$ 10 ns) with the 318, 543 and 709 keV transitions associated only with the higher-energy isomer. It should be noted that Yates *et al.* [32] identify a transition at 317.4 $\pm$ 0.4 keV feeding into the 5^- level, but the present 318.4$\pm$0.2 keV transition is considered to be distinct from this. We tentatively place the 318, 543 and 709 keV transitions above the known [32] 14 ns isomer, though there is insufficient statistical precision to confirm this from the expected delayed-coincidence relationship with the transitions below that isomer. Rather, the transitions above the 14 ns isomer are ordered so as to be consistent with comparable observations [41] for ^{198}Pt following deep-inelastic reactions.

The half-life of 14.0 $\pm$ 0.6 ns determined for the lower isomer agrees with the previous value of 14.3 $\pm$ 0.6 ns [32], as discussed in sect. 2. The upper isomer is found to have a half-life of 10.3 $\pm$ 2.4 ns (see fig. 10 insert). It is also interpreted as decaying by a low-energy, highly converted transition, as only in this way can its survival through the FRS be explained. The 90 keV upper limit for the transition energy corresponds to the one-electron K-binding energy (see also sects. 2 and 4). To our knowledge, this is the shortest-lived isomer yet observed as a primary product of projectile fragmentation.

The "semidecoupled" [44] 2-particle configuration of the 7^- isomer has already been discussed [32] in the context of the platinum systematics, but the relative amplitudes of the proton and neutron components are not known. As proposed below, in connection with ^{201}Pt and ^{202}Pt, a consistent interpretation favours 2-proton dominance, probably $h_{11/2} \otimes d_{3/2}$.

Although we do not have sufficient information to determine the character of the upper isomer, the high excitation energy, taken with the several additional decay transitions, suggests a high-spin ($J \approx 12$) configuration. The systematic observation of $J^\pi = 12^+$ nanosecond isomers [39,45] of rotation-aligned neutron $(i_{13/2})^2$ structure in less neutron-rich platinum and mercury isotopes supports a similar interpretation in the present case. Over a considerable range of neutron number, there is evidently [39,45] varying competition between low-energy ($\approx$ 100 keV) $E2$ decay to an $(i_{13/2})^2$, $J^\pi = 10^+$ state, and $E1$ decay to a negative-parity, semidecoupled band. In ^{200}Pt, a low-energy, highly converted transition is required to explain the survival of the isomer through the FRS, but it is not possible to distinguish between the $E1$ and $E2$ possibilities. As with the 14 ns isomer, the transition that directly depopulates the 10 ns isomer should have an energy $E_\gamma \leq 90$ keV. This constraint is considered in more detail in sect. 4.

3.9 $^{201}_{78}$Pt$_{123}$

Gamma-ray transitions from excited states of ^{201}Pt have been observed for the first time in the present work. Owing to the strong production of ^{200}Pt, and the similarity in the isomer half-lives for ^{200}Pt and ^{201}Pt, cross-contamination was observed (see fig. 10) in the form of transitions at

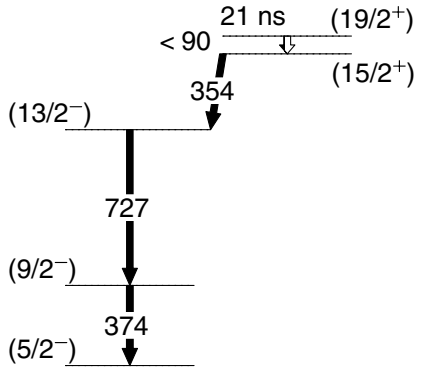

Fig. 13. Proposed level scheme for ^{201}Pt. The suggested ordering of the transitions is analogous to that of the 470-633-464 keV cascade in ^{200}Pt.

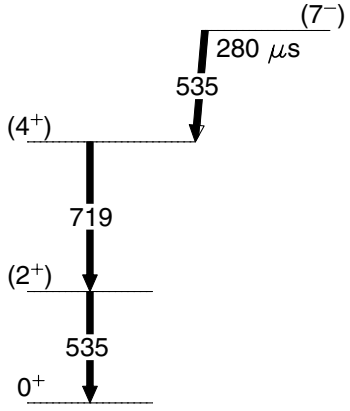

Fig. 14. Proposed level scheme for ^{202}Pt. The first two excited states are ordered so as to be consistent with the systematics of the even-even platinum isotopes. The isomer is suggested to have the same structure as the 7^- isomer in ^{200}Pt.

463.6, 470.1 and 633.0 keV. Figure 12 shows that the 354.1, 374.4 and 727.2 keV transitions are in coincidence with each other, but not with the ^{200}Pt transitions. (This gives the opportunity to quantify the contamination of an $A-1$ isotope, at the A position, which is found to be 9% of the $A-1$ intensity.) The half-life was measured to be 21 $\pm$ 3 ns, which implies (as before) that a highly converted, low-energy transition (< 90 keV) is depopulating the isomeric level. The transition-energy upper limit is discussed in sect. 4.

The known odd-mass platinum isotopes with $A \geq 189$ all have isomeric $\frac{13}{2}^+$ states, of neutron $i_{13/2}$ character, with half-lives varying from 95 μs to 4.33 days [39]. The structure that we observe could be built on either the $\frac{5}{2}^-$ ground state [39], or a long-lived $\frac{13}{2}^+$ isomer. We favour the former interpretation, on account of the high isomeric ratio of $> 32\%$ (see below). If the ordering of the transitions is analogous to that in ^{200}Pt (*i.e.* with weak coupling) then the 374 and 727 keV transitions would have $E2$ character, as illustrated in fig. 13, and the ≤ 90 keV transition depopulating the implied $\frac{19}{2}^+$ isomer would also be $E2$ (for example, $t^{\rm W}_{1/2} = 26$ μs at 50 keV, $F_{\rm W} = 0.1$). As discussed by Yates *et al.* [32], the $E2$ hindrance factor has only a weak dependence on transition energy, which is a consequence of the energy dependence of the $E2$ conversion coefficient.

This interpretation of ^{200}Pt and ^{201}Pt suggests that the 7^- configuration in ^{200}Pt is of 2-proton character, so that the coupling to the odd neutron in ^{201}Pt is not Pauli blocked. We note that Toki *et al.* [44] calculate mixed proton/neutron character for the negative-parity states of the lighter platinum isotopes, and that the energy-level systematics [39] favour increasing $h_{11/2} \otimes d_{3/2}$ 2-proton dominance with increasing neutron number, which is consistent with the interpretation given here.

The alternative possibility, that the lowest state in the cascade is of $i_{13/2}$ neutron character, leads to an implied upper-isomer spin of $\frac{27}{2}$. In this case the measured isomeric ratio of $> 32\%$ would considerably exceed the sharp-cutoff model limit of 4%.

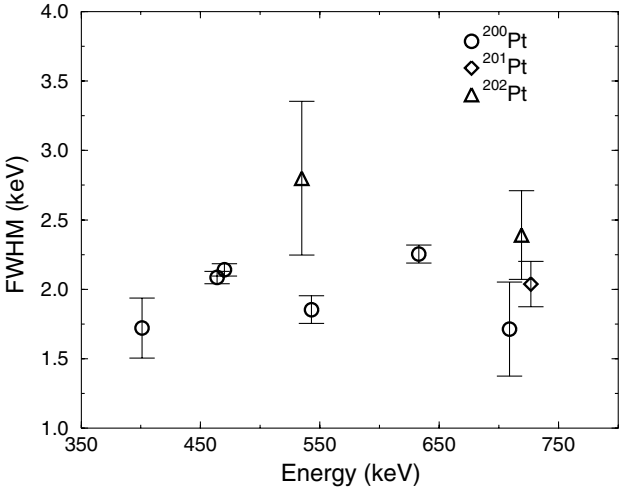

Fig. 15. Peak width (FWHM) comparison for platinum γ-ray transitions obtained in the present work. The 535 keV transition in ^{202}Pt has the highest FWHM and is suggested to be a doublet.

3.10 $^{202}_{78}$Pt$_{124}$

Unlike the short-lived ^{200,201}Pt isomers, the ^{202}Pt events spanned the full 75 μs time range. Figure 10 shows the γ-ray spectrum obtained, representing the first information on the excited states of this nuclide. The half-life of the isomer was found to be several orders of magnitude greater than those measured for ^{200}Pt and ^{201}Pt, with a value of 280^{+1800}_{-190} μs, where the upper limit corresponds to an isomeric ratio of 100%. If the sharp-cutoff limit of 35% is adopted for the isomeric ratio, then the corresponding half-life upper limit is 700 μs, so that $t_{1/2} = 280^{+420}_{-190}$ μs.

The presently proposed level sheme is shown in fig. 14. The 2^+ and 4^+ level assignments are based on the systematics of the even-even platinum isotopes (see sect. 4). The relatively large width (fig. 15) and intensity (table 1) of the γ-ray peak at 534.8 keV suggest that this is a doublet. (The intensity ratio of the 535 and 719 keV transitions is 1.84 ± 0.44.) Systematics [32,46] suggest a 7^- level as a

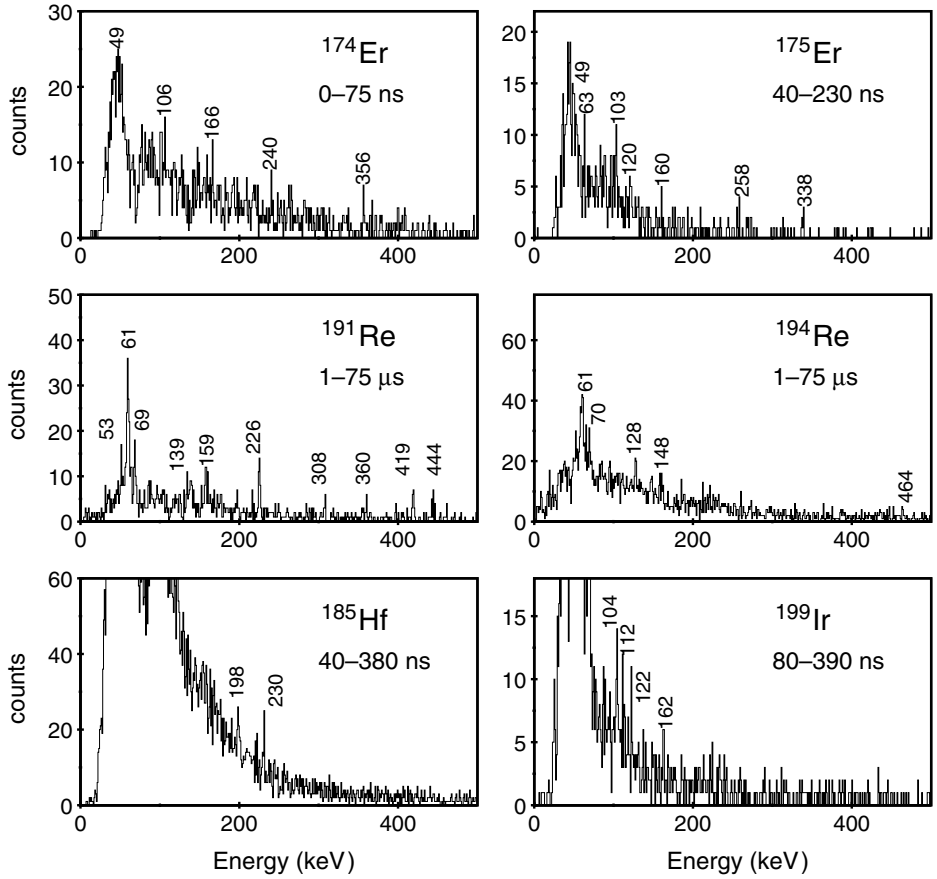

Fig. 16. Gamma-ray spectra for tentatively identified isomers. The time ranges are chosen to give the clearest spectra.

likely candidate for the isomeric state. Thus the second 535 keV transition, if it is directly depopulating the isomer, has $E3$ character ($t^{\mathrm{W}}_{1/2} = 40$ μs, $F_{\mathrm{W}} = 7$). The much longer half-life in ^{202}Pt, compared to ^{200}Pt, is seen to arise because the 7^- level presumably falls below the corresponding 5^- level, forcing $E3$ decay, compared to $E2$ decay in ^{200}Pt. The 7^- isomer is suggested to have 2-proton ($h_{11/2} \otimes d_{3/2}$) structure (cf. the interpretation of ^{201}Pt).

3.11 $^{203}_{79}$Au$_{124}$

The $\frac{3}{2}^+$ ground state of ^{203}Au has $t_{1/2} = 53$ s, and several excited states have been identified [39], but no isomers were previously established [47]. There is an $\frac{11}{2}^-$ state at 637 keV, which may be isomeric. The corresponding $\frac{11}{2}^-$ states in ^{197}Au and ^{199}Au, of $\pi h_{11/2}$ character, have half-lives of 7.7 s and 440 μs, respectively [39], but in ^{201}Au and ^{203}Au the $\frac{11}{2}^-$ state half-lives are undetermined.

The data obtained here for ^{203}Au are shown in fig. 10. A single γ-ray transition at 563.3 keV is observed. Considering the large background component, any other transitions of comparable intensity below about 200 keV would be obscured. The half-life of the 563.3 keV transition is found to be 40^{+7000}_{-20} μs, where the upper limit is determined from the isomeric ratio limit of 100%. Assuming that it directly depopulates an isomer, then the 563.3 keV transition would most likely have $E3$ multipolarity, with $F_{\mathrm{W}} \approx 1$.

It would be convenient to associate the 563.3 keV transition with the decay of the $\frac{11}{2}^-$ state in ^{203}Au. However, this does not fit with the known excited states. Accordingly, no assignment is proposed on the basis of the present data.

3.12 Other isomer candidates

Tentative evidence for isomers in a further six nuclides was found: ^{174}Er and ^{175}Er were in the fully stripped charge state of the ^{170}Dy setting; ^{191}Re and ^{194}Re were in the fully stripped charge state of the ^{191}W setting; ^{199}Ir was in the helium-like charge state of the same setting; and ^{185}Hf was in the fully stripped charge state of the ^{184}Lu setting. The γ-ray energy spectra are shown in fig. 16. In view of the considerable uncertainties in these experimental data, no interpretation is attempted. While the statistics did not permit the quantitative determination of decay half-lives, the time ranges indicated in the figure provide constraints.

4 Discussion

The reported isomers give access, in most cases, to the first spectroscopic data for the nuclide in question. The

results are collated in table 1. For any given nuclide, the present data are sparse. Nevertheless, these new data represent considerable advances, in many cases offering "stepping stones" to future study: for example, pulsed-beam experiments could exploit the new isomers in delayed coincidence, and hence determine time-correlated, in-beam transitions. It is already notable that, in the case of ^{195}Os, the assigned γ-ray transitions have been useful for nuclide identification with deep-inelastic reactions, where γ-γ coincidence relationships have been established [41]. In the following, we comment on some generic features of our results.

4.1 Isomeric ratios

The isomeric ratio is defined as the probability of populating the isomeric state in a given nuclide in the initial reaction. As part of the same research programme, we have studied the isomeric ratios of a range of known isomers [14]. In order to evaluate the experimental isomeric ratio reliably, the level scheme should be known in detail. However, the present data concern nuclides with largely unknown structure. Therefore, the quoted isomeric ratios may be subject to future revision, when more extensive spectroscopic information becomes available. Nevertheless, it is instructive to consider the values obtained. In some cases, the isomeric ratios effectively determine half-life upper limits, as discussed in sect. 3 (for ^{190}W, ^{193}Re, ^{202}Pt and ^{203}Au) or transition energy upper limits (see below).

Usually, the 100% isomeric-ratio limit greatly exceeds what could reasonably be expected. For quantitative analysis, the sharp-cutoff model gives the maximum isomeric ratio as a function of spin, based on the abrasion-ablation model of de Jong *et al.* [40]. As has been shown for well-known isomers [14], this model provides a useful isomeric-ratio upper limit, therefore enabling more stringent half-life or transition energy upper limits to be set in the present work.

When more than ten nucleons are removed from the projectile, the analytic approximation of the sharp-cutoff model may be sufficiently accurate [14]. In other cases, the code ABRABLA [40] gives an appropriate numerical estimate. For the presently studied neutron-rich nuclides, the analytic approximation is systematically found to underestimate the isomeric ratios, sometimes by large factors, in comparison with the ABRABLA code. Therefore, in the present work, all the quoted sharp-cutoff values are from the ABRABLA code. Note also that for neutron-deficient fragmentation products the analytic approximation systematically overestimates the isomeric ratios [48].

We now address those cases where there is the combination of i) a half-life much shorter than the flight time through the FRS, and ii) unobserved direct depopulation of an isomer. The relevant nuclides are ^{195}Os, ^{200}Pt (two isomers) and ^{201}Pt, where half-lives are in the range 10–26 ns. Note that, although the directly depopulating transitions are not themselves observed (according to our interpretations presented in sect. 3) the isomer production can nevertheless be determined from the conversion-corrected intensities of the γ-ray transitions that *are* observed. In these circumstances, the ion survival probability and the deduced isomeric ratios are sensitive to the conversion coefficients, and hence the energies, of the *unobserved* transitions that depopulate the isomers. As a result, the isomeric-ratio limits set conversion coefficient limits, with corresponding transition energy limits.

Consider the case of the 7^- isomer in ^{200}Pt. The γ-ray energy spectrum in fig. 10 has a high background continuum at low energies, and transitions with energies below 200 keV would not be observed in the present work. However, for the transition depopulating the 7^- isomer, a 100% upper-limit isomeric ratio requires a conversion coefficient of $\alpha_{\rm tot} \geq 5$ and, for $E2$ multipolarity, a transition energy of ≤ 100 keV. This is the same limit as set by Yates *et al.* [32]. Furthermore, if the transition energy exceeds the K-electron binding energy (90 keV for a one-electron platinum ion [37]) then the one- or two-electron ions of ^{200}Pt would have too high a probability of decaying in-flight. Therefore, we determine an upper limit of 90 keV for the transition energy in this case.

For the 10 ns upper isomer in ^{200}Pt, the decay is suggested to be of either $E2$ or $E1$ character. Independent of multipolarity, the 100% upper-limit isomeric ratio determines $\alpha_{\rm tot} \geq 2.6$. Hence, for an $E2$ transition, the energy must be ≤ 120 keV. As mentioned above, for in-flight survival of one- or two-electron ions, it can additionally be determined that the transition energy is ≤ 90 keV. For an $E1$ decay, the conversion coefficient would be relatively small, and hence there is a lower energy constraint, ≤ 30 keV, corresponding to $\alpha_{\rm tot} \geq 2.6$.

In the case of ^{201}Pt, with a tentative $E2$ assignment for the 21 ns isomer decay, the 100% isomeric-ratio upper limit determines $\alpha_{\rm tot} \geq 5$ and a transition energy ≤ 100 keV. Again, however, the energy should not exceed the one-electron K-binding energy of 90 keV.

Finally, the 26 ns isomer in ^{195}Os is determined to have $\alpha_{\rm tot} \geq 1.6$ for its decay radiation. Hence, for the different cases of $E1$, $E2$ and $M1$ radiations, the transition-energy limits are ≤ 35, ≤ 130 and ≤ 150 keV, respectively. This time the ions are fully stripped of electrons, so that the K binding energy does not provide additional constraints.

In each of these cases, the transition-energy upper limit is lower than what would have been obtained by inspection of the γ-ray energy spectrum, with its large continuum background. Also, these are conservative upper limits, as, in reality, the isomeric ratios would be considerably below 100%. To account for this, the sharp-cutoff model can be used (for given spins) to obtain the isomeric-ratio upper limits, leading to new conversion coefficient upper limits. These are compiled in table 2, along with the assumed isomer angular-momentum values and transition multipolarities. The transition energy limits for alternative multipolarities can simply be estimated from the tabulated conversion coefficient limits. In the case of ^{201}Pt, however, the ABRABLA evaluation of the isomeric-ratio upper limit (30%) is approximately the same as the experimental

Table 2. Summary of constraints on conversion coefficients and transition energies for short-lived isomers, assuming the given J^π assignments and percentage isomeric ratios (IR). The superscript *sc* refers to the sharp-cutoff upper-limit estimate.

	$t_{1/2}$	J^π	$\mathrm{IR}^{\max}$	$\alpha_{\mathrm{tot}}^{\max}$	$\mathrm{IR}^{\mathrm{sc}}$	$\alpha_{\mathrm{tot}}^{\mathrm{sc}}$	λ	$E_\gamma^{\max}$	E_γ^{sc}
^{195}Os	26 ns	–	100	≥ 1.6	–	–	$E1$	≤ 35	–
							$M1$	≤ 150	–
^{200}Pt	14 ns	7^-	100	≥ 5	36	≥ 50	$E2$	≤ 90	≤ 60
^{200}Pt	10 ns	12^+	100	≥ 2.6	8	≥ 25	$E2$	≤ 90	≤ 70
							$E1$	≤ 30	≤ 8
^{201}Pt	21 ns	$\frac{19}{2}^+$	100	≥ 5	30	–	$E2$	≤ 90	–

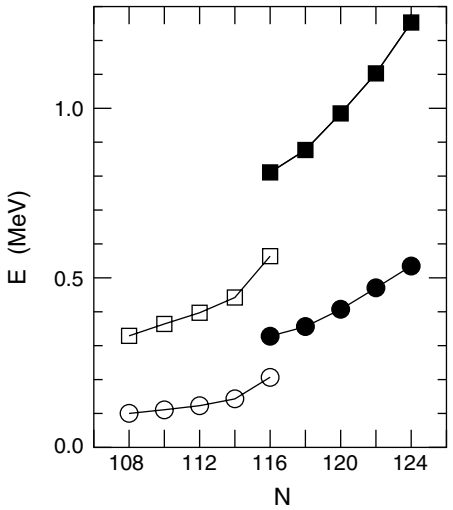

Fig. 17. Energies of the first 2^+ states (circles) and 4^+ states (squares) as a function of neutron number for $Z = 74$ tungsten isotopes (open symbols) and $Z = 78$ platinum isotopes (filled). The data for the highest neutron numbers of each element are from the present work. Other values are from ref. [39].

lower limit (32%). While, in principle, this implies a large conversion coefficient ($\alpha_{\mathrm{tot}} \gg 5$) the present information does not provide a useful quantitative estimate.

4.2 Collective behaviour in even-even nuclei

Simple measures of nuclear collectivity come from excited-state energies of even-even nuclides, such as the energy of the first 2^+ state, $E(2^+)$, and the energy ratio $E(4^+)/E(2^+)$ [49,50]. We now have new data to determine these energies for the even-even nuclides ^{190}W and ^{202}Pt. The behaviour of $E(2^+)$ and $E(4^+)$ is shown for the tungsten and platinum isotopes in fig. 17. Although $^{202}\mathrm{Pt}_{124}$ follows systematic trends, the energies of the $^{190}\mathrm{W}_{116}$ levels can be seen to be slightly higher than might have been expected from simple extrapolations. The nuclide ^{190}W is located in the prolate-oblate transition region between well-deformed and spherical nuclei, which makes its behaviour of particular interest. There could also be some influence from the proposed $Z = 76$ subshell closure [51]. This situation has been discussed in our earlier paper [12]. The clarification of the apparent subshell effect requires new data for other neutron-rich nuclides in this mass region.

5 Summary

Decays from nanosecond to millisecond isomers have been observed in the neutron-rich $A \approx 190$ region using relativistic projectile fragmentation of a ^{208}Pb beam at 1 GeV per nucleon on a beryllium target. The fragments were separated and identified using the FRS spectrometer. This enabled their mass and charge to be determined before they were stopped at the final focus, where time-correlated, delayed γ-ray events were recorded by germanium detectors. Nuclide identification was unambiguous. A total of 12 new isomers with half-lives in the range 10 ns $\rightarrow$ 1 ms have been discussed, corresponding to 11 different nuclides: ^{188}Ta, ^{190}W, ^{192}Re, ^{193}Re, ^{195}Os, ^{197}Ir, ^{198}Ir, ^{200}Pt, ^{201}Pt, ^{202}Pt and ^{203}Au. In addition, tenetative evidence for isomers in ^{174}Er, ^{175}Er, ^{185}Hf, ^{191}Re, ^{194}Re and ^{199}Ir was shown, as well as evidence for fragmentation events corresponding to the previously unreported nuclides ^{197}Os, ^{200}Ir and ^{170}Dy.

The nuclides ^{200}Pt and ^{201}Pt presented the combination of the shortest-lived isomers studied here, and sufficient intensity to benefit from γ-γ coincidences. With a half-life of only 10.3 ± 2.4 ns, the newly found isomer in ^{200}Pt represents the shortest-lived isomer to be transported (on account of its much longer in-flight half-life) through a magnetic spectrometer.

While the spectroscopic information obtained in the present work is limited, the isomers themselves may provide valuable stepping stones for future detailed studies.

The excellent work of the SIS synchrotron staff providing a high-intensity primary beam is acknowledged. We thank K-H. Behr, A. Brünle and K. Burkhard for their valuable FRS technical support. This work received financial support from the UK Engineering and Physical Sciences Research Council, Polish Committee of Scientific Research under grant KBN 2 P03B 036 15, USA Department of Energy contracts DE-FG02-96ER40983 and 91ER40609, EU Access to Large Scale Facilities Programme, and Swedish Natural Sciences Research Council. The clover detectors were funded by CEA (France), EPSRC (UK), GSI (Germany) and NBI (Denmark). We are grateful to G. Sletten for the use of the NBI EXOGAM clover detector. D.M.C. acknowledges the support of an Advanced Fellowship AF/100225 from the EPSRC.

References

1. R. Schneider *et al.*, Z. Phys. A **348**, 241 (1994).
2. Ch. Engelmann *et al.*, Z. Phys. A **352**, 351 (1995).
3. M. Bernas *et al.*, Phys. Lett. B **415**, 111 (1997).
4. R. Grzywacz *et al.*, Phys. Lett. B **355**, 439 (1995).
5. R. Grzywacz *et al.*, Phys. Rev. C **55**, 1126 (1997).
6. C. Chandler *et al.*, Phys. Rev. C **56**, R2924 (1997).
7. R. Grzywacz *et al.*, Phys. Rev. Lett. **81**, 766 (1998).
8. J.M. Daugas *et al.*, Phys. Lett. B **476**, 213 (2000).
9. C. Chandler *et al.*, Phys. Rev. C **61**, 044309 (2000).
10. E. Bouchez *et al.*, Phys. Rev. Lett. **90**, 082502 (2003).
11. M. Pfützner *et al.*, Phys. Lett. B **444**, 32 (1998).
12. Zs. Podolyák *et al.*, Phys. Lett. B **491**, 225 (2000).
13. M.N. Mineva *et al.*, Eur. Phys. J. A **11**, 9 (2001).
14. M. Pfützner *et al.*, Phys. Rev. C **65**, 064604 (2002).
15. S. Åberg, Nucl. Phys. A **306**, 89 (1978).
16. F.R. Xu, P.M. Walker, R. Wyss, Phys. Rev. C **62**, 014301 (2000).
17. P.M. Walker, G.D. Dracoulis, Hyperfine Interact. **135**, 83 (2001).
18. M. Pfützner *et al.*, *Proceedings of the International Conference on Experimental Nuclear Physics in Europe, Sevilla, Spain, 1999*, edited by B. Rubio, M. Lozano, W. Gelletly, AIP Conf. Proc. **495**, 113 (1999).
19. Zs. Podolyák *et al.*, *Proceedings of the 2nd International Conference on Fission and Properties of Neutron-Rich Nuclei, St. Andrews, Scotland, 1999*, edited by J.H. Hamilton, W.R. Phillips, H.K. Carter (World Scientific, London, 2000) p. 156.
20. Zs. Podolyák *et al.*, *Proceedings of the International Conference on the Structure of the Nucleus at the Dawn of the Century, Bologna, Italy, 2000*, edited by G.C. Bonsignori, M. Bruno, A. Ventura, D. Vretenar (World Scientific, 2001) p. 298.
21. C. Schlegel *et al.*, Phys. Scr. **T88**, 72 (2000).
22. M. Caamaño *et al.*, Nucl. Phys. A **682**, 223c (2001).
23. M. Caamaño *et al.*, Acta Phys. Pol. B **32**, 763 (2001).
24. P. Mayet *et al.*, *Proceedings of the International Conference on Nuclear Physics at the Border Lines, Lipari, Italy, 2001*, edited by G. Fazio, G. Giardina, F. Hanappe, G.Immé, N. Rowley (World Scientific, 2002) p. 193.
25. Zs. Podolyák *et al.*, *Proceedings of the International Conference on Exotic Nuclei at the Proton Drip Line, Camerino, Italy, 2001*, edited by C.M. Petrache, G. Lo Bianco (University of Camerino, 2002) p. 189.
26. P. Mayet *et al.*, *International Nuclear Physics Conference, Berkeley, USA, 2001*, edited by P. Fallon *et al.*, AIP Conf. Proc. **610**, 761 (2002).
27. Zs. Podolyák *et al.*, Prog. Theor. Phys. **146**, 467 (2002).
28. Zs. Podolyák *et al.*, Nucl. Phys. A **722**, 273c (2003).
29. M. Pfützner, P.H. Regan, P.M. Walker, Zs. Podolyàk, M. Caamaño, J. Gerl, M. Hellström, P. Mayet, M. Mineva, Acta Phys. Pol. B **32**, 2507 (2001).
30. H. Geissel *et al.*, Nucl. Instrum. Methods in Phys. Res. B **70**, 286 (1992).
31. C. Scheidenberger, Th. Stöhlker, W.E. Meyerhof, H. Geissel, P.H. Mokler, B. Blank, Nucl. Instrum. Methods Phys. Res. B **142**, 441 (1998).
32. S.W. Yates, E.M. Baum, E.A. Henry, L.G. Mann, N. Roy, A. Aprahamian, R.A. Meyer, R. Estep, Phys. Rev. C **37**, 1889 (1988).
33. J.A. Becker *et al.*, Phys. Rev. C **26**, 914 (1982).
34. G.J. Lane *et al.*, Nucl. Phys. A **682**, 71c (2001).
35. B. Fornal *et al.*, Phys. Rev. Lett. **87**, 212501 (2001).
36. F. Rösel, H.M. Fries, K. Alder, H.C. Pauli, At. Data Nucl. Data Tables **21**, 91 (1978).
37. W.R. Johnson, G. Soff, At. Data Nucl. Data Tables **33**, 405 (1985).
38. K.E.G. Löbner, Phys. Lett. B **26**, 369 (1968).
39. R.B. Firestone, V.S. Shirley (Editors), *Table of Isotopes*, 8th edition (Wiley, New York, 1996).
40. M. de Jong, A.V. Ignatyuk, K.H. Schmidt, Nucl. Phys. A **613**, 435 (1997).
41. J.J. Valiente-Dobón *et al.*, to be published.
42. J.A. Cizewski, D.G. Burke, E.R. Flynn, R.E. Brown, J.W. Sunier, Phys. Rev. C **27**, 1040 (1983).
43. J.A. Cizewski, E.R. Flynn, R.E. Brown, D.L. Hanson, S.D. Orbesen, J.W. Sunier, Phys. Rev. C **23**, 1453 (1981).
44. H. Toki, K. Neergård, P. Vogel, A. Faessler, Nucl. Phys. A **279**, 1 (1977).
45. C. Günther, H. Hübel, A. Kleinrahm, D. Mertin, B. Richter, W.D. Schneider, R. Tischler, Phys. Rev. C **15**, 1298 (1977).
46. P. Schüler, J. Recht, H. Wilzek, K. Hardt, C. Günther, K.P. Blume, K. Euler, V. Kölschbach, Z. Phys. A **317**, 313 (1984).
47. S. Rab, Nucl. Data Sheets **70**, 173 (1993).
48. K.A. Gladnishki *et al.*, Phys. Rev. C **69**, 024617 (2004).
49. R.F. Casten, W. Frank, P. Von Brentano, Nucl. Phys. A **444**, 133 (1985).
50. R.F. Casten, Phys. Rev. C **33**, 1819 (1986).
51. H. Mach, Phys. Lett. B **185**, 20 (1987).